Bull Volcanol (2006) 68: 549–566
DOI 10.1007/s00445-005-0029-2

RESEARCH ARTICLE

T. Shimano · S. Nakada

Vesiculation path of ascending magma in the 1983 and the 2000 eruptions of Miyakejima volcano, Japan

Received: 19 August 2004 / Accepted: 31 August 2005 / Published online: 11 January 2006

Abstract The vesiculation of magma during the 1983 eruption of Miyakejima Volcano, Japan, is discussed based on systematic investigations of water content, vesicularity, and bubble size distribution for the products. The eruption is characterized by simultaneous lava effusion and explosive sub-plinian ('dry') eruptions with phreatomagmatic ('wet') explosions. The magmas are homogeneous in composition (basaltic andesite) and in initial water content ($H_2O = 3.9 \pm 0.9$ wt%), and residual groundmass water contents for all eruption styles are low (H_2O <0.4 wt%) suggestive of extensive dehydration of magma.

For the scoria erupted during simultaneous 'dry' and 'wet' explosive eruptions, inverse correlation was observed between vesicularity and residual water content. This relation can be explained by equilibrium exsolution and expansion of ca. 0.3 wt% H_2O at shallow level with different times of quenching, and suggests that each scoria with different vesicularity, which was quenched at a different time, provides a snapshot of the vesiculation process near the point of fragmentation. The bubble size distribution (BSD) varies systematically with vesicularity, and total bubble number density reaches a maximum value at vesicularity $\Phi \sim 0.5$. At $\Phi \sim 0.5$, a large number of bubbles are connected with each other, and the average thickness of bubble walls reaches the minimum value below which they would rupture. These facts suggest that vesiculation advanced by nucleation and growth of bubbles when $\Phi < 0.5$, and then by expansion of large bubbles with coalescence of small ones for $\Phi > 0.5$, when bubble connection becomes effective.

Low vesicularity and low residual water content of lava and spatter ($\Phi < 0.1$, $H_2O < 0.1$ wt%), and systematic decrease in bubble number density from scoria through spatter to lava with decrease in vesicularity suggest that effusive eruption is a consequence of complete degassing by bubble coalescence and separation from magma at shallow levels when magma ascent rate is slow.

Keywords Eruption style · Basaltic magma · Degassing · Water content · Vesicularity · BSD · Coalescence

Editorial responsibility: J. Stix

T. Shimano (✉) · S. Nakada
Earthquake Research Institute, University of Tokyo,
1-1-1 Yayoi, Bunkyo-ku, Tokyo, 113-0032, Japan
e-mail: shimano@cneas.tohoku.ac.jp

Present address:
T. Shimano
Center for Northeast Asian Studies, Tohoku University,
41 Kawauchi, Aoba-ku,
Sendai City, Miyagi 980-8576, Japan

Introduction

Conduit flow models have shown that eruption style is mainly controlled by interplay of two processes of magma during ascent, "vesiculation" and "gas loss" (Jaupart and Allegre 1991; Woods and Koyaguchi 1994). Effusive eruption is a consequence of extensive gas loss as opposed to explosive eruption. However, these models cannot yet predict the full range of eruption styles, probably due to failure of critical assumptions or oversimplification of the two processes. These models assume vesiculation to be independent of some factors that might affect the results considerably (e.g., size distributions and connectivity of bubbles), and gas loss to depend only on the permeability and pressure gradients in the wall rocks. Such processes are not easy to assess from natural observations designed to test these assumptions.

In this respect, bubble growth models may help us to understand vesiculation of magma because elemental processes might be recorded in the products. A model assuming constant nucleation and growth rates of bubbles has been applied to bubble size distributions (BSDs) of natural samples to estimate the ascent rate of magma (Mangan et al. 1993; Klug and Cashman 1994; Mangan and Cashman 1996). Other models showed that nucleation occurs sporadically rather than constantly, and that nucleation and growth rate can be controlled by the degree of supersaturation as well as physical properties such as melt viscosity and volatile diffusivity around bubbles (e.g., Proussevitch

et al. 1993a; Toramaru 1995; Proussevitch and Sahagian 1998; Lensky et al. 2001). These improved models are also quantitatively consistent with experiments (Liu and Zhang 2000). However, textures in natural samples are much more complex and may record other processes excluded in the models above (size dependence on bubble growth rate, bubble–bubble interaction, gas loss, etc.). Thus, to model the ascent of magma, we must understand what the products really record, and clarify the dominant process which may change in the course of vesiculation during ascent.

The 1983 and the 2000 eruptions of Miyakejima volcano, Japan, are two of the best documented eruptions on the basis of direct observation, geophysical monitoring, and stratigraphical investigation (Aramaki and Hayakawa 1984; Hayakawa et al. 1984; Aramaki et al. 1986; Nakada et al. 2005; Kaneko et al. 2005). In this paper, we discuss the vesiculation path of magma during ascent in relation to eruption styles, on the basis of a systematic investigation of water contents and vesicular structure of the products.

Summary of eruptions

Miyakejima volcano is located ca. 180 km south of Tokyo, Japan (Fig. 1). It is one of the most active volcanoes in the northern part of the Izu-Mariana volcanic arc, and has erupted every several tens of years in historical time (1469, 1535, 1595, 1712, 1763–69, 1811, 1835, 1874, 1940, 1962; Tsukui et al. 2001). The 1983 eruption took place on the southwestern flank of Mt. Oyama, and lasted for about 9 h. The sequence of eruption was recorded in detail by the mass media, Japan Coast Guard (JCG) and Japan Self Defense Forces (JSDF). The 2000 eruption started as a subaqueous eruption occurred in the sea on the western flank (Kaneko et al. 2005), and was followed by summit eruptions which formed a new caldera (Geshi et al. 2002; Nakada et al. 2005). Although summit eruptions constitute the main phase of the 2000 eruption, only the submarine eruption is discussed here for the 2000 eruption because of the different petrological features of the products of the summit eruption.

To discuss eruption style quantitatively, we use V_G/V_L, the volumetric flux ratio of gas to magma (Fig. 2). Most data are obtained as follows. V_L is obtained as time averaged value using total erupted volume, duration of the phenomenon, and the cross section area of vent. V_G is estimated from the height of fountain h by assuming velocity of ballistics v at vent represents minimum velocity of gas phase which throws out the ballistics, and $v = (2gh)^{1/2}$, where g is acceleration of gravity. Despite a large error up to one order of magnitude (factor of 2; Vergniolle and Mangan 2000), we use this ratio because it is one of a few measurable values for eruption phenomena. Previously, the ratio has been estimated for some eruptions (ca. 70 and 10^5 for Hawaiian and Strombolian eruptions, respectively; Vergniolle and Mangan 2000). This ratio is also useful because we can discuss the relationship between this ratio and v_g/v_l, the volume ratio of bubbles to solid of the products, if we regard v_g/v_l as an instantaneous volume flux at the time magma solidified and at some level or part of magma in the conduit. In addition, the ratio v_g/v_l is more sensitive than vesicularity Φ to changes above $\Phi \sim 0.7$ (Gardner et al. 1996) which is common for explosive eruptions.

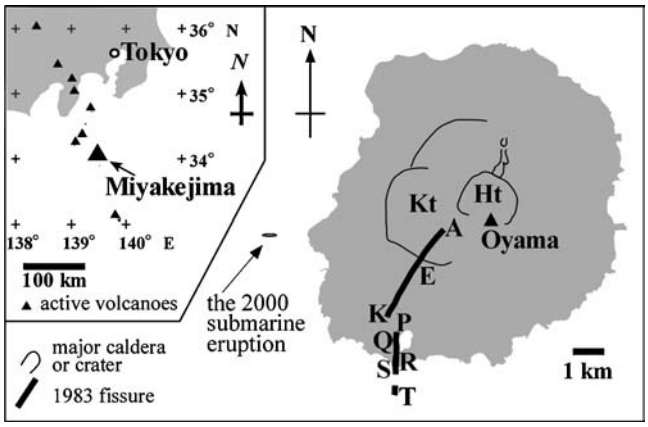

Fig. 1 Locality map of Miyakejima Volcano. The 1983 eruption occurred on the southwestern flank of Mt. Oyama. The 2000 submarine eruption occurred in the sea ca. 1 km west of Miyakejima (ca. 80 m below sea level). Ht: Hatcho-taira caldera, Kt: Kuranoki-taira caldera

The 1983 eruption

The 1983 eruption is characterized by fissure eruptions on the southwestern flank of Mt. Oyama, and littoral explosions in the vicinity of the seashore. The fissure is ca. 4.5 km long with 16 discrete vent segments, A to K and P to T, from north to south (Fig. 1). The eruption sequence is divided into 5 stages in terms of locality, time, and style of eruption (Table 1; Stage 1 to 5; Aramaki and Hayakawa 1984; Aramaki et al. 1986). Hereafter, unit PQ7, for example, stands for 7th unit in ascending order that is formed by products from vents P to Q, and PQ7 stands for its constituents (Endo et al. 1984; Sumita 1985).

Stage 1 is characterized by simultaneous lava flow effusion (4.65×10^6 m^3 DRE) and fountaining and subplinian eruptions (1.56×10^6 m^3; column height >3,000 m; Hayakawa et al. 1984). The eruption started at the intersection of the fissure and outline of Kuwanoki-taira

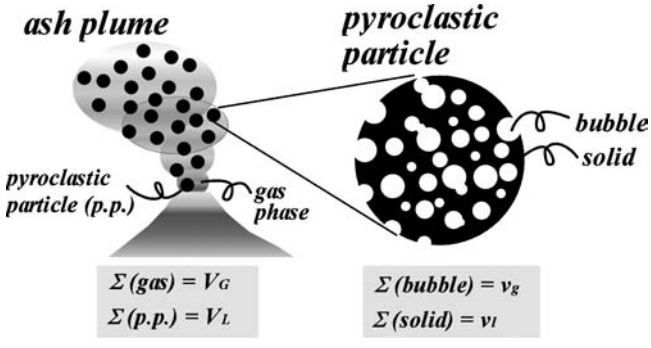

Fig. 2 Schematic illustration of the relationships between solid (liquid) and gas volumes in ash plume and in pyroclastic particles. See text for details

Table 1 Time sequence of the 1983 eruption of Miyakejima Volcano (stratigraphical data are from Endo et al. 1984, and Sumita 1985)

	Stage	Time	Characteristic eruption style	Major active vents	Total erupted mass (x 10^6 m^3 DRE)		Average eruption rate (m^3/s)		Average V_G/V_L		Unit (measured)
					explosive	effusive	explosive	effusive	explosive	effusive	
time ↓	Stage 1	15:15–16:38	Fountaining, Strombolian, sub-Plinian, lava effusion	A–K	0.37	4.65	~10^3	~10^1	10^1–10^3	~ 10^1	A2-3
	Stage 2	16:38–19:17	Phreatomagmatic explosion, fountaining, sub-Plinian, lava effusion	P–S	PQ: 1.43 RS: 0.61*	Very small volume	~10^2	Very small rate	10^1–10^2	?	R2, S2*
	Stage 3	19:17–21:26	Phreatomagmatic explosion	PQ	1.50	–	?	–	?	–	–
	Stage 4	21:26–22:33	Fountaining, sub-Plinian, phreatomagmatic explosion	K,R	0.04	–	?	–	>10^2	–	R3-5
	Stage 5	22:33–6:00 (Nov. 4)	Sporadic fountaining	P, R,	Very small volume	–	?	–	?	–	–
				total	8.60						

*S2 deposit may have formed in stage 4 (Aramaki et al. 1986)

caldera (Locality E in Fig. 1), and the fissure extended both north and south at a nearly constant propagation rate of 26–40 m/min. The eruption along vent A to vent K lasted for about 1 h. The average eruption rate is ca. 10^3 m^3/s (Aramaki and Hayakawa 1984). The length and width of the solidified dike from vent A to vent K are ca. 2.9 km and ca. 0.3 m, respectively. Thus the average magma volume flux per unit cross section is ca. 10^{-1} to 10^0 m /s. The gas eruption speed is estimated to be at least ca. 50 m/s, if we assume fountain height h ($h > 100$ m; Aramaki and Hayakawa 1984) represents initial velocity of ballistics that were thrown out by gas jet at the vent, and use $v = (2gh)^{1/2}$. The volumetric flux ratio of gas to magma V_G/V_L is estimated 10^1 to 10^3.[1]

Stage 2 is characterized by phreatomagmatic eruption on the southern side of Miyakejima simultaneous with fountaining (also with temporal sub-plinian eruption), generating dense and vesicular scoria, respectively (units PQ1 to 6, R1 to 2, S1 to 2; Sumita 1985). The fissure propagated from vent P to the sea (vent R to vent T). The eruption lasted for about 90 min (The activity at vent T was very short). The volume of magma erupted at vents R and S is 1.18 × 10^6 m^3 (0.70 ×10^6 m^3 as a tuff ring; Hayakawa et al. 1984). The average eruption rate was ca. 10^2 m^3/s, and the average magma flux per unit cross section area of dike (length ca. 100 m × width 0.3 m) was V_L ~10^0 m/s. The fountain height at vent R was ca. 50 to 200 m. As fountain heights reached h ~200 m, the gas velocity was at least ca. 10^1 to 10^2 m/s, and V_G/V_L is ca. 10^1 to 10^2.

Stage 3 is characterized by phreatomagmatic eruption with ejection of large bombs at vents P and Q (PQ7, 8). The total volume of magma from the two vents is 1.46 ×10^6 m^3 (Hayakawa et al. 1984).

Stage 4 is characterized by major eruption at vent R (R3 to R5). The erupted volume at vent R at this stage was 0.27 ×10^6 m^3 (Hayakawa et al. 1984).

Stage 5 is characterized by sporadic and weak fountaining at vents P and R after a strong earthquake of magnitude 6.2 (units PQ9 and R6). The eruption had stopped by ca. 6:00 of October 4.

We obtained little observation of phenomenological values such as discharge rates or fountaining heights for Stage 3 to Stage 5 because of dark condition at night. Thus, in the present study, samples mainly from vents A to K at Stage 1 and from vents R and S at Stage 2 were investigated because of good correlation between phenomena and deposit (Endo et al. 1984; Sumita 1985). Samples after Stage 3 were investigated only for large explosive eruptions that resulted in broad distribution of airfall deposits.

The 2000 submarine eruption

The 2000 submarine eruption is characterized by spatter cone formation, or strombolian-like eruption, in the sea about 1 km west of Miyakejima, and by discolored seawater emerging as several batches of circular plumes (each size ca. 10 m in diameter; Fig. 2a in Kaneko et al. 2005) consisting of gas bubbles and silicic precipitates. The eruption lasted for 20 to 40 min. The volume of each plume (radius r) is calculated $4/3\pi r^3$ ~10^2 to 10^4 m^3 assuming spherical geometry of the plume (i.e., 10^3 to 10^5 m^3 if summed up for all batches). Several pyroclastic cones (diameter ca. 20 to 100 m, height ca. 2 to 3 m) which consist mostly of fresh essential spatter and scoria were formed on the seafloor (Kaneko et al. 2005). Distribution of the essential materials is limited in the vicinity of the cone, and total volume of erupted magma is estimated on the order of 10^3 m^3. Thus, the volumetric ratio of gas to magma, averaged V_G/V_L, is

[1] For lava flows the ratio of gas to magma volume should be less than ca. 10^1 judging from the apparent density of the most vesicular solidified lava.

Table 2 Samples investigated in this study

	Eruption style	Sample name	Year	Vent	Stage	Unit
Explosive	Dry (fountaining, strombolian, sub-plinian)	A2-3 dry scoria, A2-3 dry spatter	1983	A	1–2	A2-3
		R2 dry scoria, R2 agglutinate	1983	R	2	R2
		R3-5 dry scoria	1983	R	4	R3-5
	Wet (phreatomagmatic, submarine)	S2 wet scoria	1983	S	2	S2
		2k wet scoria	2000	–	–	–
Effusive		AK1 lava	1983	A-K	1	A2-3
		R2 lava	1983	R	2	R2

on the order of 1 to 10^2. Hereafter, samples for the 2000 submarine eruption are named as 2k scoria and spatter.

Samples

Samples investigated in the present study can be classified into mainly three types of products; dry scoria (+spatter) produced by explosive eruption on land, wet scoria (+spatter) produced by explosive eruption under water or by phreatomagmatic eruption on seashore, and lava flow produced by effusive eruption on land (Table 2). We define 'wet' for the products in the sea or phreatomagmatic eruptions, and 'dry' for the products of eruptions on land without phreatomagmatic explosions.

A2-3 dry scoria and spatter were generated by fountaining and strombolian eruption during a very short period (Stage 1). R2 dry scoria and spatter were generated mainly by fountaining with sub-plinian ash column above (Stage 2). R3-5 dry scoria was produced mainly by sub-plinian eruption, probably associated with a high eruption column (several km), judging from its broad distribution (Stage 4). The dry scoria are highly vesicular, and the spatter are less vesicular (Fig. 3).

S2 wet scoria was produced by phreatomagmatic eruptions that formed a tuff ring, which occurred almost simultaneously with the activity of R2. Vesicularity of the scoria is low on average, but variable and some grains are highly vesicular similar to R2 dry scoria.

AK1 lava erupted from fissure from vent A to vent K during Stage 1 simultaneously with A2-3 dry scoria. R2 lava is very small lava flow (ca. 10 m long, < 5 m thick) which erupted simultaneously with R2 dry scoria. R2 agglutinate was produced in the proximal area of vent R during Stage 2. The lavas and the agglutinate are dense compared with scoria and spatter.

2k wet scoria and spatter were produced by the 2000 submarine eruption. Pieces of spatter are several tens of centimeters in diameter, and have a vesicular core surrounded by a 1- to 2-cm-thick dense bread crust. The crust has surface with many open cracks and wrinkles. The spatter is very fragile due to the cracks. Most 2k wet scoria were generated by breakage of the crust judging from their size (1 to 2 cm), relatively high density, and angular shape. The scoria have a relatively wide range in vesicularity similar to S2 wet scoria.

Analytical methods

Chemical composition

Whole rock compositions were determined by XRF spectrometer (Philips PW2400) at Earthquake Research Institute, University of Tokyo (ERI). Glass, Groundmass (glass + microlites) and phenocryst compositions were determined by EPMA (JEOL8800R) at ERI under conditions of 15 kV and 12 nA. The glass and groundmass compositions were estimated by averaging analyses using a 10 to 20 μm defocused beam. The number of analyses used for averaging is listed in Table 3. Phenocryst compositions were determined for each spot using a focused beam (ca. 1 μm). The groundmass SiO_2 content of aphyric samples with many microlites of plagioclase and pyroxene was identical to the whole rock composition within 1 wt%.

Residual water content

Residual water contents of samples were analyzed at ERI by the Karl-Fisher titration method (Turek et al. 1976; Westrich 1987) with a coulometric hygrometer (Mitsubishi Chemical Co.). Powder samples were prepared by hand crushing. At least several grams of sample were crushed, homogenized, and separated to check reproducibility by analyzing several portions of powder. For each analysis, ca. 200 mg of sample was used. Water was extracted by two-step heating with dry N_2 carrier gas; first at 120±20°C for adsorbed water, and second at 1,000±20°C for dissolved water. Some samples were analyzed with CuO powder to assess the loss of H_2O by dehydration in the form of H_2, which was reported for amphibole dehydration (Miyagi et al. 1998), and there was no significant difference from the case without CuO. The reproducibility of several analyses for a single sample is better than 0.1 wt%. Bulk rock water contents were converted to groundmass water content by using the total phenocryst mode.

Vesicularity

Vesicularity of all samples was measured by the "glass beads" method (Sasaki and Katsui 1981) as follows.

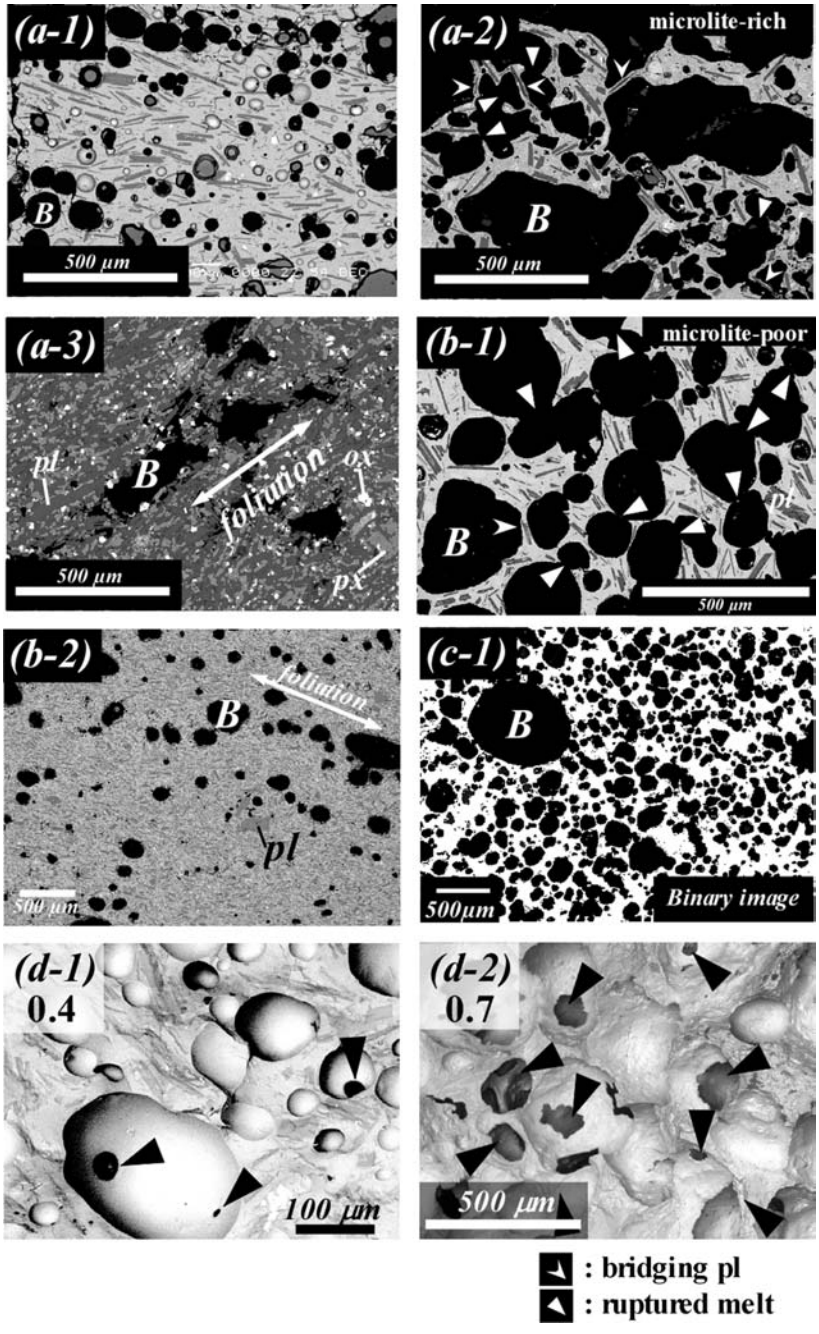

Fig. 3 BEIs of sample of the 1983 eruption from (a) vents R to S; (a-1) S2 wet scoria, (a-2) R3-5 dry scoria, (a-3) R2 lava flow. (b) vents A to K; (b-1) A2-3 dry scoria, (b-2) A2-3 dry spatter. (c) (c-1) Binary image of scoria of the 2000 submarine eruption. (d) 3D images of scoria by SEM. (d-1) 2k wet scoria by the 2000 eruption ($\Phi \sim 0.4$), (d-2) A2-3 dry scoria by the 1983 dry eruption ($\Phi \sim 0.7$). Triangles and arrows indicate apertures and bridging plagioclase microlites between bubbles, respectively. B: bubble, pl: plagioclase

Volume of sample (solid + pore) is estimated by subtracting the volume of packed glass beads in a measuring cylinder alone from volume of packed glass beads and sample. Glass beads were all sorted to 0.5–0.7 mm in diameter to treat them smoothly. Volumes were measured in measuring cylinder with glass beads of ca. 1/5 of the full cylinder volume (50 or 100 ml depending on sample size). Statistical error for more than 15 measurements is <10% relative to the average sample volume. Samples were measured without a paraffin coat to measure residual water content afterwards. The underestimation in volumes of samples with bubbles larger than bead grains (0.5–0.7 mm) due to invasion of glass beads is less than 10% relative to the average volume.

Connectivity

Connectivity of bubbles $C^{\#}$ is defined here as volume fraction of connected bubbles to all bubbles;

$$C^{\#} = \frac{V_{\text{connected-bubbles}}}{V_{\text{all-bubbles}}} \quad (1)$$

The volume of all bubbles can be estimated using the volumes of solid + all bubbles and solid alone. The volume of solid + all bubbles of the sample is measured by the glass beads method. The volume of solid is calculated from sample weight and solid density (2,700 kg/m^3). The volume of connected bubbles can be estimated by subtracting

Table 3 Whole rock, groundmass, glass chemical compositions, and modal composition of the products

No.	1	2	3	4	5	6	7	8	9
Year	1983	1983	1983	1983	1983	1983	1983	1983	2000
Unit	S2	R3-5	R3-5	R3-5	R2	R2	A2-3	A2-3	2k
Category	Wet scoria	Dry scoria	Dry scoria	Dry scoria	Agglutinate	Lava	Dry scoria	Dry spatter	Wet scoria
wholerock (wt%)									
SiO_2	51.75	–	53.67	53.31	51.83	51.92	53.71	53.89	53.66
TiO_2	1.19	–	1.29	1.28	1.19	1.30	1.38	1.39	1.36
Al_2O_3	15.56	–	15.32	15.22	15.57	14.82	14.57	14.54	14.77
FeOt	12.63	–	12.24	12.27	12.63	13.22	13.05	13.15	12.97
MnO	0.23	–	0.23	0.23	0.23	0.24	0.24	0.24	0.24
MgO	5.12	–	4.03	4.13	5.11	4.95	4.10	4.13	4.00
CaO	10.02	–	8.86	8.86	10.01	9.69	8.60	8.68	8.83
Na_2O	2.53	–	2.80	2.83	2.57	2.59	2.84	2.86	2.81
K_2O	0.36	–	0.54	0.54	0.34	0.46	0.55	0.56	0.56
P_2O_5	0.11	–	0.15	0.15	0.11	0.14	0.16	0.16	0.15
Total	99.51	–	99.11	98.80	99.58	99.33	99.18	99.60	99.35
groundmass (wt%)									
n*	71	112	64	102	51	228	30	171	266
SiO_2	53.33	54.69	56.22	56.53	53.01	55.38	55.58	55.99	54.93
TiO_2	0.60	1.74	1.41	1.51	0.60	0.39	1.67	1.32	1.35
Al_2O_3	17.77	13.92	14.44	13.02	18.70	18.07	13.71	14.28	14.84
FeO	9.25	14.49	12.68	13.84	8.42	7.68	14.34	12.34	12.59
MnO	0.22	0.11	0.00	0.26	0.19	0.19	0.25	0.25	0.24
MgO	4.61	3.24	3.78	4.55	4.51	4.19	3.47	3.66	3.84
CaO	11.29	8.33	8.48	7.15	11.55	10.76	7.89	8.65	8.79
Na_2O	2.64	2.74	2.35	2.37	2.73	2.88	2.36	2.50	2.78
K_2O	0.24	0.61	0.50	0.66	0.25	0.41	0.52	0.88	0.52
P_2O_5	0.05	0.14	0.14	0.11	0.03	0.05	0.22	0.12	0.11
glass (wt%)									
n*	12	13	23	16	18	23	6	9	112
SiO_2	59.47	57.02	57.42	58.00	97.75	81.88	56.19	58.40	55.96
TiO_2	3.94	3.24	1.85	1.84	0.14	0.50	1.92	2.28	1.91
Al_2O_3	8.54	10.88	12.94	12.97	1.09	10.79	12.43	11.26	12.17
FeO	18.44	18.30	14.48	15.92	0.34	0.93	16.58	17.08	15.60
MnO	0.00	0.00	0.27	0.25	0.01	0.02	0.25	0.29	0.28
MgO	0.27	0.93	2.96	2.81	0.02	0.02	2.68	1.16	2.93
CaO	5.42	5.93	7.34	5.39	0.17	1.70	7.23	6.13	7.69
Na_2O	1.76	2.18	1.93	1.79	0.30	2.34	2.08	2.24	2.54
K_2O	1.07	1.19	0.65	0.91	0.05	1.68	0.49	0.97	0.76
P_2O_5	1.08	0.34	0.16	0.12	0.13	0.15	0.15	0.19	0.16
total	99.39	100.70	97.50	97.56	101.66	99.03	98.70	98.82	97.47
Mode (vol%)									
P1	0.5	3.6	–	3.9	2.5	0.1	–	–	3.6
ol	tr	tr	–	tr	0.2	tr	–	–	0.1
cpx	0.2	tr	–	0.3	tr	0.1	–	–	0.2
opx	tr	tr	–	tr	tr	tr	–	–	0.1
mt	tr	tr	–	tr	tr	tr	–	–	tr
groundmass	99.3	96.4	–	95.8	97.3	99.8	–	–	96.1
groundmass crystallinity (wt%)**	20–30	~30		~30	~75	~80	< 20	~45	20–35

*Number of analyses for groundmass and glass compositions

**Groundmass crystallinity is calculated by least square regression using compositions of microlites, groundmass, and glass. tr: traceable amount

the volume of solid + isolate bubbles, V_{pyc}, from that of solid + all bubbles which is measured by the glass beads method. V_{pyc} was estimated by pycnometry using a helium pycnometer (Accu Pyc 1330; Shimadzu Co. Ltd.) in the Department of Geosystem Science, Nihon University, which measures the pressure difference before and after the input of sample into a chamber of known volume. The effect of temperature change is calculated by the gas equation. The pressure difference is small (0.3 MPa), and no significant sample damage was observed after this analysis, although there are damaged samples for vesicular samples even before the analysis.

Bubble number density and size distributions

Bubble size data were obtained from thin sections (e.g., Cashman and Mangan 1994). BEIs (backscattered electron images; grayscale bitmap files) of samples were converted to binary images, and analyzed by free software (NIH image). BEIs of ×18, ×35, ×100, ×250, and ×500 were taken at ERI under 15 kV by Secondary Electron Microprobe (JEOL5600) in order to obtain a sufficient number of bubbles and to get a suitable resolution of small bubbles. Each image consists of 1260 × 960 pixels with 8 bit data. To avoid artifacts no modification was made to the decoalesced image (Toramaru 1990). The threshold in a gray scale spectrum to make a binary file was set between the peaks of bubbles and other phases. Two dimensional (2D) bubble size was represented by the diameter of a circle with an equivalent area to the analyzed bubble. The 2D size distribution was converted to 3D size distribution using the method of Sahagian and Proussevitch (1998). The results are of the same order of magnitude, and relative relations in number density are consistent with those using the conversion method of Cashman and Mangan (1994).

Results

Whole rock composition and crystal content

The 1983 ejecta investigated in the present study are homogeneous aphyric basaltic andesite with SiO_2 ~52–55 wt% (Table 3, Fig. 4). The total phenocryst content is <5 vol%. Phenocrysts are euhedral to subhedral and consist of plagioclase, hypersthene, augite, magnetite, and trace amounts of olivine. The amounts of microlites calculated by least squares regression are variable (less than 20 to more than 80 vol%). Microlites consist of plagioclase, pyroxene, and Fe-Ti oxides. The ejecta of the 2000 submarine eruption are basaltic andesite close in composition to the 1983 products (Kaneko et al. 2005). The phenocryst assemblage is also the same as the 1983 ejecta. The groundmass crystallinity of the 1983 A2-3 dry scoria (<20 vol%) is slightly lower than the scoria of the 2000 submarine and the 1983 eruptions at vents R and S.

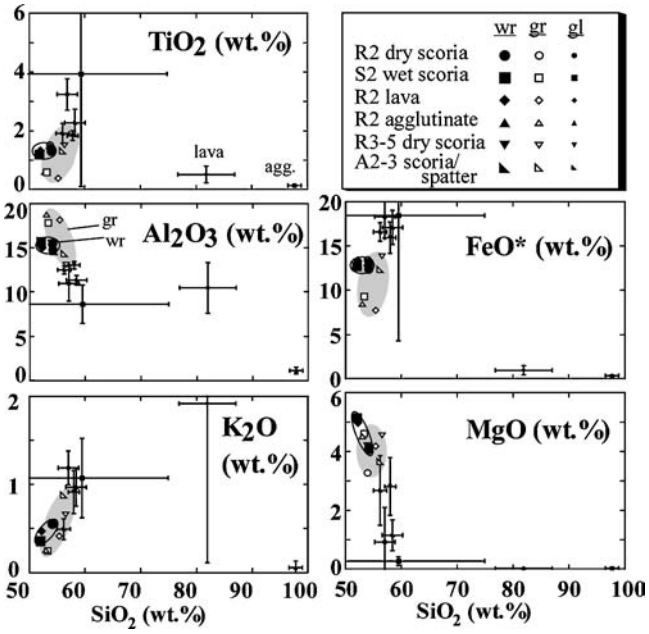

Fig. 4 Whole rock, groundmass, and glass compositions of the ejecta of the 1983 Miyakejima eruption. Error bars (1σ) are within symbols for whole rock compositions, whereas error bars for groundmass compositions are similar to those of glasses (they are not shown for clarity). Whole rock and groundmass (average) compositions are almost identical regardless of eruption styles. Glass compositions of lava and agglutinate are highly silicic due to high crystallinity

Groundmass and crystal compositions

The groundmass compositions (Fig. 4; Table 3) are homogeneous for the products of different eruption styles in the 1983 eruption (SiO_2 ~53–56 wt%) and for those in the 2000 submarine eruption (SiO_2 ~55–56 wt%). Compositions of crystals are also similar among different products (Fig. 5). Most core compositions of plagioclase phenocrysts range from An 80 to 90 with a peak at about An 85 (Fig. 5a). Cores of some crystals with An >90 are considered to be of accidental origin, because of their unusual occurrence (large size, aggregated texture, multiple cores in a single crystal, corroded dusty zoning). The rims of plagioclase phenocrysts range from An 55 to 85, with a peak at about An 65–75. The maximum An content of microlites (65–70) is similar to that of the phenocryst rims. Pyroxene phenocrysts have a similar composition range for all eruption styles in the formula of Lindsley (1983; Fig. 5b), and the rim-pairs give magma temperatures of ca. 1,100°C (QUIlF program; Frost and Lindsley 1993). Aphyric samples contain pyroxene microlites whose composition range is similar to porphyritic samples.

Groundmass water content, vesicularity, and connectivity

Groundmass residual water content (H_2O_{gr}), vesicularity (Φ), volumetric ratio of vesicle to solid (v_g/v_l; Fig. 2), and

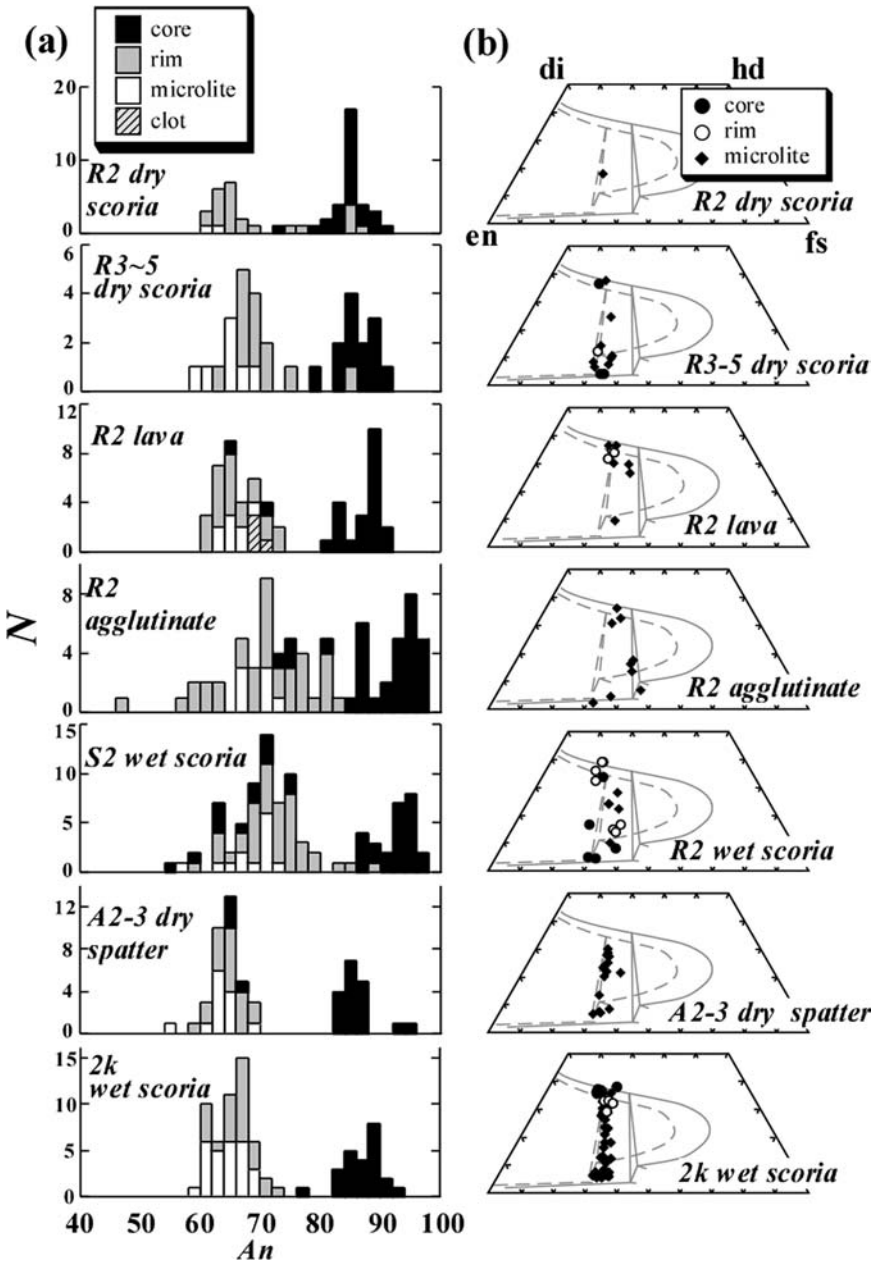

Fig. 5 Compositions of plagioclase and pyroxenes of the 1983 and of the 2000 submarine products. (**a**) plagioclase. N is the number of crystals analyzed. (**b**) pyroxenes. di: diopside, hd: hedenbergite, en: enstatite, and fs: ferrosilite. Solid and broken lines indicate isotherms of 1100 and 1000°C (Lindsley, 1983)

connectivity ($C^{\#}$) are shown in Table 4. Residual water contents do not correlate with sample size (Fig. 6a) precluding significant vesiculation after fragmentation. Water contents of all samples are less than 0.4 wt%. The ejecta of phreatomagmatic and submarine eruptions (wet scoria) have systematically higher water contents (0.2–0.4 wt%) than dry scoria of 'dry' explosive eruptions (0.1–0.2 wt%; Fig. 6b). Water contents of lava flows and spatter are a little lower than the dry scoria (0–0.2 wt%). Vesicularity of the wet scoria (0–0.4; $v_g/v_l = 0.3$–2) are systematically lower than most of the dry scoria (0.5–0.8; $v_g/v_l = 1$–4). Connectivity of all samples is high ($C^{\#} > 0.9$; Table 4). Even lava flow samples with vesicularity less than 0.5 have high connectivity.

BSD and bubble shapes

Volume fraction of bubbles

Bubbles larger than 1 mm occupy up to more than 50% of the total volume of bubbles in A2-3 dry scoria, A2-3 dry spatter, and R3-5 dry scoria (Fig. 7). The volumetric size distribution is bimodal with peaks at less than 0.2 mm and at ca. 0.5–0.7 mm in S2 and 2k wet scoria (Fig. 7). The volume fraction of bubbles less than 0.4 mm is dominant in R2 lava.

Table 4 Groundmass residual water content (H_2O_{gr}), vesicularity (Φ), volumetric ratio of vesicles to solid (v_g/v_l), connectivity ($C^{\#}$), and total bubble number density N_T of the product. n.a.: not analyzed

Year	Crater	Sample name	H_2O_{gr} (wt%)		Vesicularity Φ		v_g/v_l	Connectivity $C^{\#}$		N_T ($\times 10^6$ cm^{-3})
			Range	Avg.	Range	Avg.		Range	Avg.	
1983	A	A2-3 dry scoria	0.13	0.13	0.6–0.7	0.631	1.71	>0.85	0.98	1–2
1983	A	A2-3 dry spatter	0.06–0.10	0.08	0.1–0.2	0.129	0.15	ca. 1		<1
1983	A-K	AK1 lava	<0.1	0.10	<0.1	n.a.	n.a.	n.a.	n.a.	2–3
1983	S	S2 wet scoria	0.10–0.34	0.26	0.2–0.7	0.449	0.95	n.a.	n.a.	6–11
1983	R	R2 dry scoria	0.13	0.13	0.6–0.7	0.706	2.4	ca. 1		2–8
1983	R	R3-5 dry scoria	0.14	0.14	ca. 0.7	0.72	2.58	n.a.	n.a.	–
1983	R	R2 lava	<0.1	0.1	<0.1	0.063	0.07	ca. 1		2–4
1983	R	R2 agglutinate	<0.1	ca. 0	<0.1	0.023	0.02	ca. 1		–
2000	–	2k wet scoria	0.22–0.32	0.26	0.2–0.5	0.34	0.56	>0.86	0.98	6–12

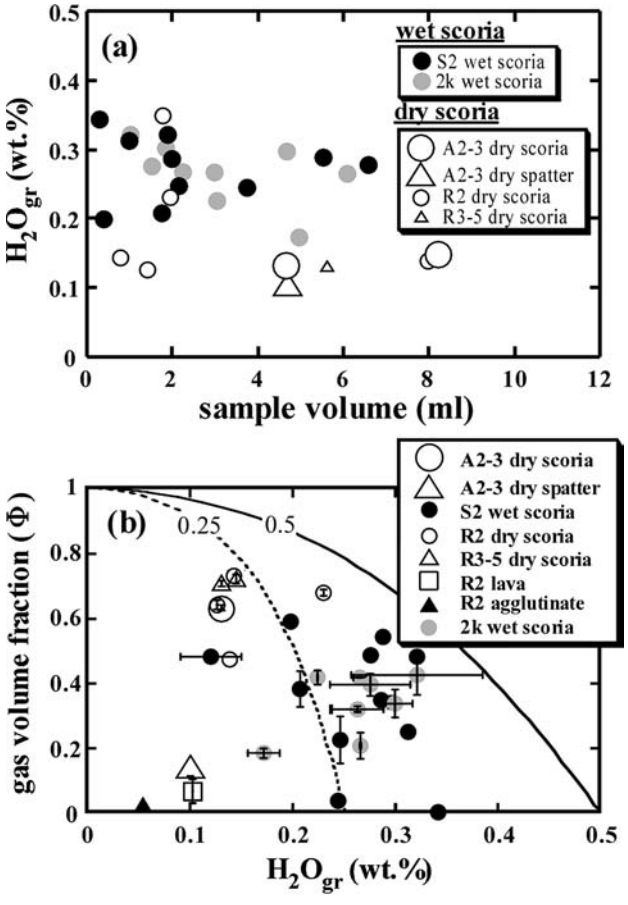

Fig. 6 **a** Sample weight and water content (H_2O_{gr}) of the 'wet' and 'dry' scoria of the 1983 eruption. **b** Residual water content (H_2O_{gr}) and vesicularity (Φ) of the 1983 products and the 2000 submarine ejecta. Error bars for some samples are within the symbols. Solid and broken lines indicate equilibrium vesiculation path in closed system with water content of 0.5 and 0.25 wt%, respectively

Total number density

The total bubble number density N_T of A2-3 dry scoria is ca. 1–2 $\times 10^6$ cm^{-3}, whereas those of A2-3 dry spatter is a little smaller and in the order of 10^5 to 10^6 cm^{-3}. The total number density of R2 dry scoria is ca. 2–8 $\times 10^6$ cm^{-3}. The total bubble number density of S2 and 2k wet scoria are higher than those of the dry scoria, and are ca. 6–11 $\times 10^6$ cm^{-3} and ca. 6–12 $\times 10^6$ cm^{-3}, respectively. The total number density of R2 lava is ca. 2–4 $\times 10^6$ cm^{-3}.

The form of BSD plots

To compare with the constant nucleation and growth model (e.g., Mangan et al. 1993), d-log N_v plots are shown in Fig. 8. N_v is the number density of bubbles in the bin range. The BSDs of most samples consist of two segments with different slopes in the range of bubble size d < 4 mm; a steep slope for diameters d < 0.5 mm (Seg-I), and a moderate slope for d > 0.5 mm (Seg-II). Only one segment is observed for lavas (Seg-I). In the range d < 0.4 mm, however, BSDs of all samples cannot be fit by only an exponential function, but consist of several segments with different slopes (Fig. 8b).

To compare with other models such as power law models (e.g., Blower et al. 2001), bi-logarithmic plots are shown in Fig. 9. Note that vertical axis shows sum of the number density larger than d. This minimizes meaningless zigzags of BSDs due to artifacts in setting bin size of BSDs (Blower et al. 2001). S2 and 2k wet scoria are enriched in small bubbles (d < 0.1 mm). The number density of larger bubbles (d > 0.1 mm) differs from grain to grain, and is well correlated with vesicularity; the higher the vesicularity, the higher the number density of the large bubbles (Fig. 9a). On the other hand, the number density of small bubbles remains nearly constant. In addition, the number density of large bubbles becomes constant when vesicularity Φ reaches ca. 0.5 (dashed line in Fig. 9). For Φ > 0.5 number density of all bubble size classes increases very little. R2 dry scoria has a similar form of BSD compared to the most vesicular sample among S2 wet scoria (Fig. 9b).

A2-3 dry scoria is depleted in small bubbles (d < 0.1 mm, especially less than a few tens of micrometers; Fig. 9b). A2-3 dry spatter is more depleted in small bubbles (d < 0.4 mm), but number density of large classes (d > 0.4 mm) is similar to that of scoria. R2 and AK1 lavas are depleted also in large bubbles (Fig. 9b).

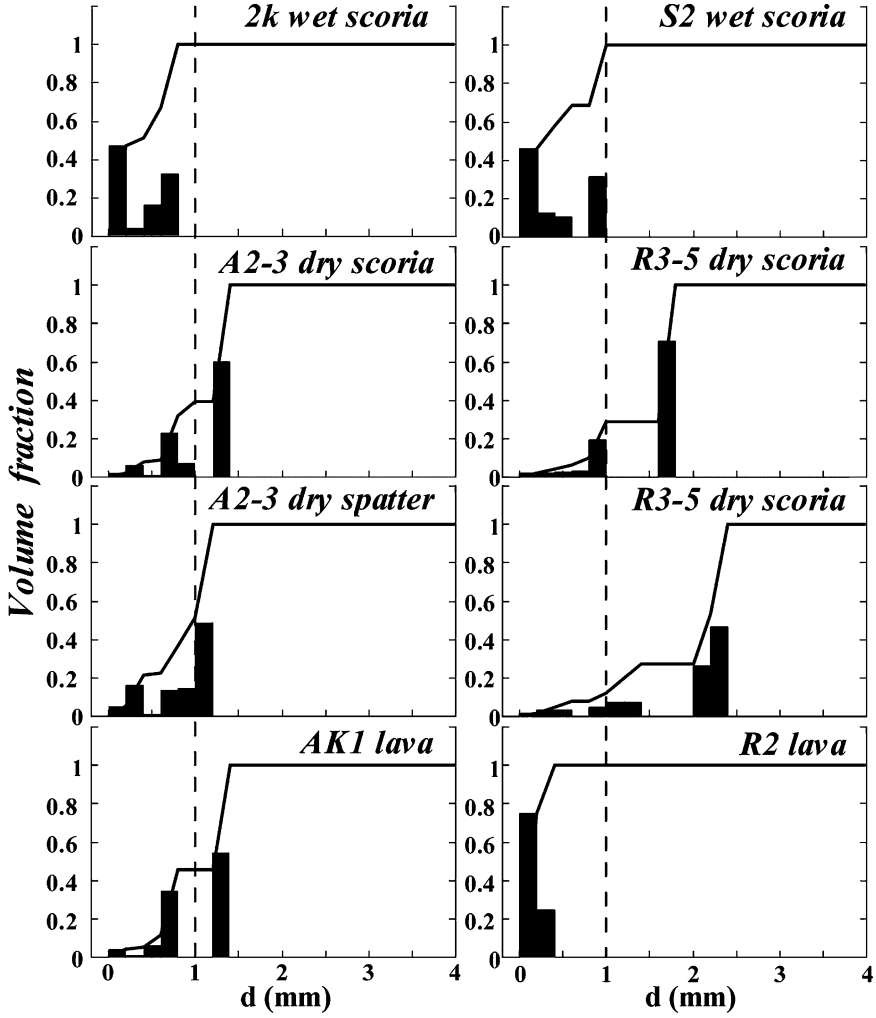

Fig. 7 Bubble size distribution in volume fraction of the products of the 1983 and the 2000 submarine eruption (d < 4 mm). Solid lines show cumulative volume fraction of bubbles less than d

Bubble shapes

Most bubbles in scoria samples are spherical to subspherical.

In S2 and 2k wet scoria (microlite-rich), the spatial distribution of bubbles is heterogeneous (Fig. 3a-1). Most large bubbles are connected with each other at a few points (Fig. 3d-1), but small bubbles are distributed homogeneously and are isolated. Microlites are enclosed in glass in the less vesicular parts, whereas they modify bubble shape (polygonal shape) in the highly vesicular parts of the scoria.

In R2 and R3-5 dry scoria (microlite-rich), bubbles larger than 1 mm are polygonal or irregular and concave inward suggesting they were pushed from the outside by smaller bubbles (Fig. 3a-2). Some microlites modify bubble shape, and bridge melt acting as a part of bubble wall.

In A2-3 scoria (microlite-poor), melt films near the point of contact between two bubbles are often ruptured, and some are retracted with smooth surfaces (Fig. 3b-1). Small bubbles (<10 μm) tend to occur between the larger ones without being connected with each other. Microlites are enclosed in glass, and do not modify bubble shape.

Bubbles in spatter and lava are ellipsoidal and distributed heterogeneously, forming foliation parallel to the bottom side of the lava or agglutinate (Fig. 3a-3 and 3b-2). Some bubbles have aspect ratios up to ca. 1:10. Most microlites are enclosed in glass, but some modify bubble shape due to high microlite content and depletion of melt (Fig. 3a-3).

Initial conditions at the onset of magma ascent

Composition of plagioclase just before the eruption

Water contents of magma in a chamber just before eruption (initial H_2O content) have been estimated by several methods (Johnson et al. 1994; Mertzbacher and Eggler 1984; Rutherford and Devine 1996; Anderson et al. 1989). In the present study, the initial water content was estimated by the petrological hygrometer of Housh and Luhr (1991) because the hygrometer of Mertzbacher and Eggler (1984) is limited to a narrow range of composition and mineral assemblage (Schmitt and De Silva 2000), and melt inclusions are ambiguous as to the time and place of entrapment, in addition to unavailability of large melt inclusions required for analysis.

To estimate water contents by the hygrometer, temperature, pressure, plagioclase composition, melt composition,

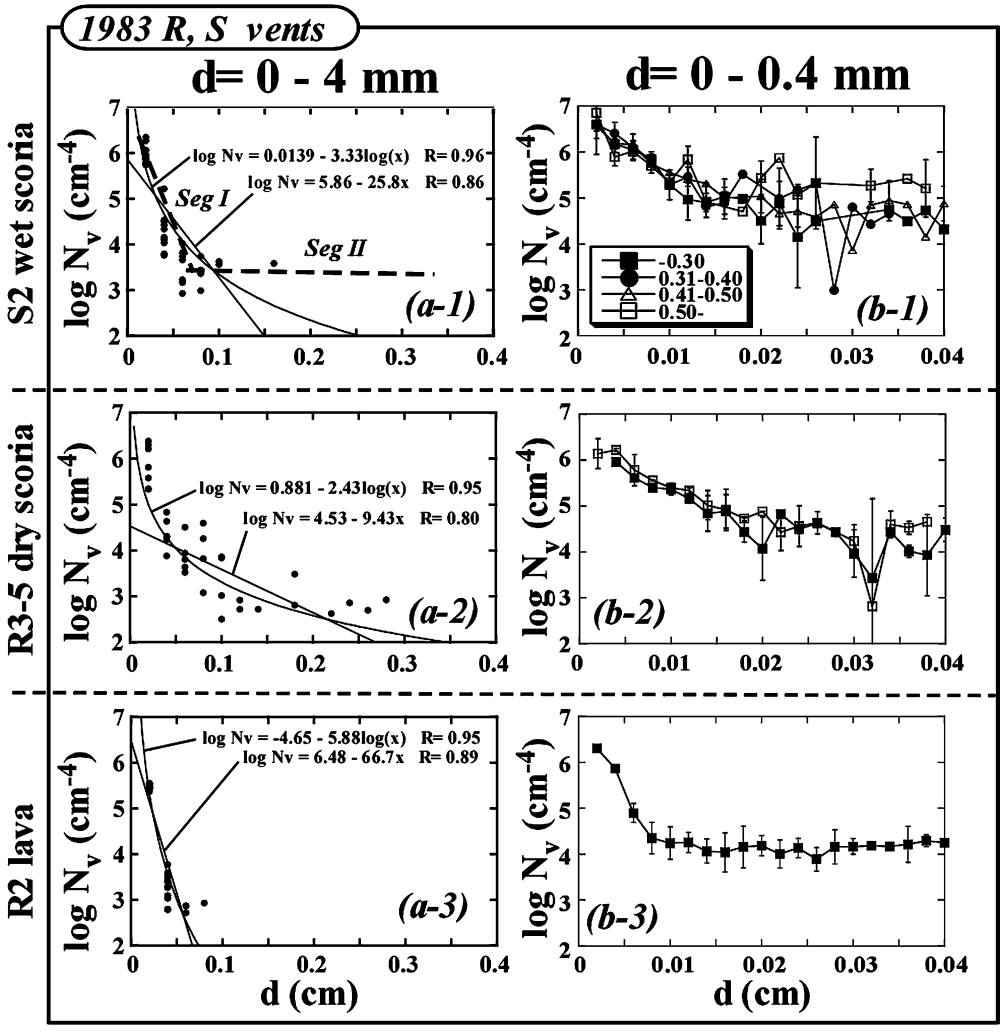

Fig. 8 Bubble size distribution of the products of the 1983 eruption (at vent R) in linear diameter and logarithmic number density units. N_v is bubble number density in each bin range. **a** $d < 4$ mm; Two segments of slope are observed; Seg I: steep slope in the range $d < 0.5$ mm, and Seg II: gentle slope in the range $d > 0.5$ mm. Linear line: fit by an exponential function, Curve line: by a power law function. The BSDs may be better fit by power law than by (truncated) exponential function. **b** $d < 0.4$ mm; The BSDs are not linear but seems to be consisted by several segments. The BSDs in (b-1) are for samples with different vesicularity ranges as shown in legend

and fO_2 at the time of interest are required independently. Pressure and fO_2 are set 200 MPa, and NNO (+0 to +1), respectively (Yasuda et al. 2001).

The outermost rims of plagioclase phenocryst have skeletal and dendritic textures with compositions similar to the microlites. Such dendritic texture is typical also for pyroxene microlites which show cotectic crystallization with plagioclase microlites. Compositions of microlite pyroxenes fall in the miscibility gap between orthopyroxene and clinopyroxene phenocrysts (Fig. 5b). These facts indicate that the outermost rims of phenocrysts and microlites were rapidly crystallized under disequilibrium conditions (Lofgren 1980) such as super-cooling by ascent. Thus, we conclude that the inner rim, a zone several tens of micrometers inside the outermost rim of the phenocryst, was in equilibrium with melt at the onset of magma ascent.

Initial water content

The hygrometer is applied to plagioclase compositions at different positions between the core and outermost rim of the phenocrysts, each as a pair with the groundmass composition (Fig. 10). Temperature just before eruption was set at 1,100°C (Fig. 5b). The calculated H_2O contents for both An and Ab component substitutions are identical (indicating equilibrium) when plagioclase compositions of inner rim were selected. In contrast, H_2O contents for the outermost rims and cores of phenocrysts, and microlites are not the same. This reinforces the idea that the inner rims of phenocrysts were in equilibrium with melt of groundmass composition.

The initial H_2O contents of magma, were estimated to be 3.9 ± 0.9 and 3.7±0.3 wt%, for the 1983 and the 2000 submarine products, respectively. Therefore, the initial water contents are identical within analytical error (ca. 1 wt% H_2O) for different eruption styles. This is consistent with the water content of some melt inclusions of the 2000 submarine products analyzed by micro-FTIR (ca. 3 wt%; A. Yasuda, pers. com.). The water content of 3.7–3.9 wt% is the solubility at ca. 130 MPa (Moore et al. 1998), corresponding to lithostatic pressure at a depth of ca. 5–6 km. This overlaps with the depth range of hypocenters of seismic activity just after the 1983 eruption and before the 2000 eruption, which are closely related to magmatic activity (Ueki et al. 1984; Fujita et al. 2001). Thus, it is suggested

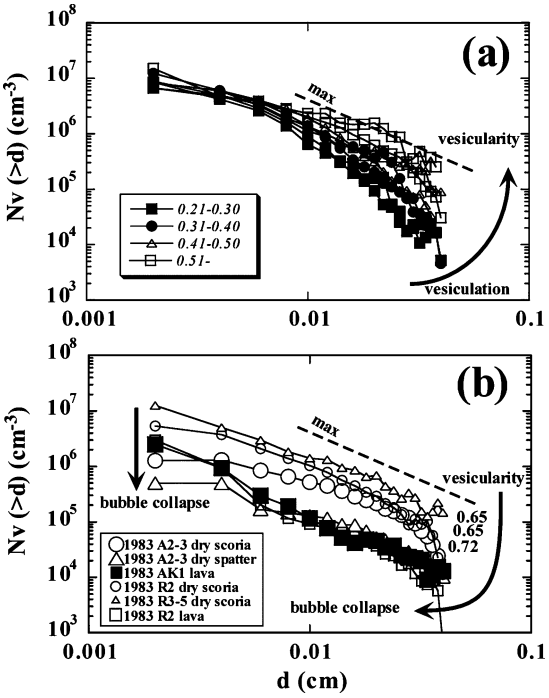

Fig. 9 BSD and vesicularity among products of different eruption styles in cumulative bi-logarithmic units. N_v (>d) is bubble number density in the range larger than d. (**a**) wet scoria. The number density of large (>0.1 mm) bubbles increases as vesicularity increases when $\Phi < 0.5$, whereas the number density of small bubbles is fixed. When $\Phi > 0.5$, the number density of large bubbles increases no more (broken line with "max"). (**b**) dry scoria, spatter, and lava flow. The number density of small sizes decreases with increase in vesicularity for scoria, whereas the number density of all sizes decreases with decrease in vesicularity of spatter and lava flows

that the magma was located at a depth of ca. 5–6 km before the eruptions.

Degassing path

As the initial magmatic conditions were almost identical for different eruption styles (dry explosive and effusive), eruption style should have been controlled either (1) by a slight difference in initial conditions or (2) by the vesiculation and/or degassing process during ascent from the magma chamber to the surface. As phreatomagmatic eruptions are affected by seawater and aquifer conditions, we only discuss the difference between dry explosive and effusive eruptions. However, as the products by wet explosive eruptions are generated simultaneously with dry eruptions, we treat them as they experienced similar vesiculation processes except for quench by external water.

Amount of exsolved water

We must evaluate the amount of exsolved water (ΔH_2O) because the major driving force for an explosive eruption is the exsolution and expansion of water. ΔH_2O can be estimated by subtracting the residual groundmass water content (H_2O_{gr}) from the initial water content (H_2O_i). As H_2O_{gr} for all juvenile materials are less than 0.4 wt%, the ΔH_2O are all more than 3 wt%, ca. 90% of the initial water content H_2O_i (Fig. 6). This fact indicates that exsolution of H_2O was large during ascent, and that the difference in the amount of exsolved water (ΔH_2O) for different eruption styles is very small relative to the initial water content. As the volume of ca. 3 wt% of H_2O at 0.1 MPa becomes up to several thousand times that of magma, all eruption styles should have been explosive (i.e., V_G/V_L = ca. 10^3) if all the exsolved water had taken part in the eruption. This is inconsistent with the observed diversity of eruption styles, and thus it is suggested that difference in the behavior of volatiles during ascent is a major cause of the diversity.

Where is eruption style controlled?

In contrast to the uniformity in initial water content and amount of exsolved water, the residual water content (H_2O_{gr}) and vesicularity of the ejecta (Φ) vary systematically among different eruption styles (Fig. 6b). Dry scoria have lower water contents and higher vesicularity than wet scoria. The volume ratio, v_g/v_l ($= \Phi/\{1-\Phi\}$), of dry scoria is twice that of wet scoria. Both vesicularity and water content of lava flows and spatter are lower than the other erupted materials.

The variation in vesicularity and H_2O_{gr} of scoria in explosive eruptions can be accounted for by closed system vesiculation of ca. 0.3 wt% of water at shallow depths without disequilibrium in exsolution and expansion (<300 m; Fig. 6b). No sample with residual water content higher than 0.4 wt% is found. Scoria of some wet explosive eruptions have vesicularity as low as $\Phi < 0.2$. Even these dense scoria occasionally have large but deformed bubbles ($d >$ 1 mm) indicating they have grown at depths and survived from gas loss while most large bubbles have been separated.

Judging from these observations, it is suggested that exsolution and gas loss was intensive enough at the deeper levels, and that eruption style or generation of scoria is controlled by the manner of gas loss at a shallow level, where vesicularity can change only by a small amount of water exsolution (<0.4 wt%).

Gas segregation and loss

Then, does the vesicular texture represent the whole amount of vapor in the ash plumes at the exit of vent (before entrainment of air), or only a part of it? Two extreme cases are possible. (1) The gas inside the ash column at the vent originated from gas phase already separated out of magma during ascent at deeper levels (>300 m; bubbles with arrows in Fig. 13). The gas originated from remnant bubbles in the pyroclasts makes only a minor contribution to the eruption. (2) All the gas inside the ash column at the vent can be accounted for by bubbles in the products. The discrepancy in volume ratios between the ash column, V_G/V_L, and the products, v_g/v_l, is explained by expansion

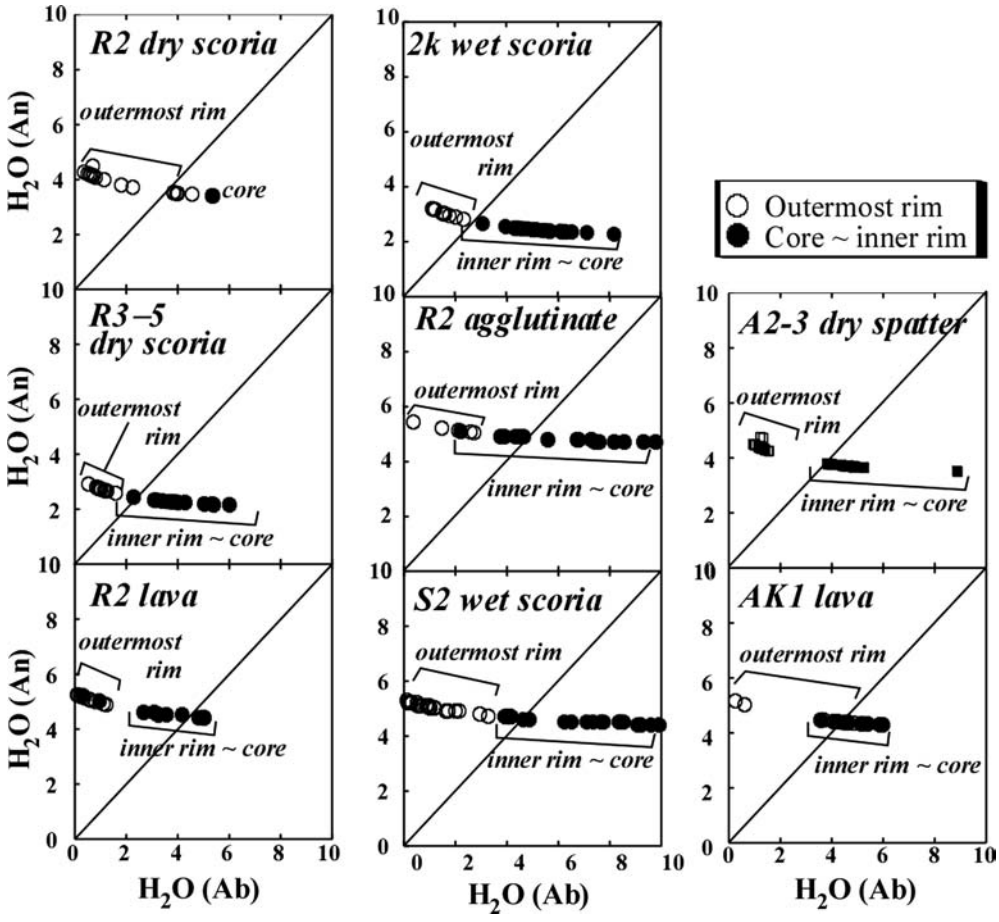

Fig. 10 Results of the hygrometer by Housh and Luhr (1991) for the products in the 1983 and the 2000 submarine eruptions. Results are shown for composition pairs of groundmass and phenocryst plagioclase from core to the outermost rim at a temperature of 1,100°C. The results of two reactions (for An and Ab components; H_2O(An) and H_2O(Ab)) are identical when plagioclase at inner rim is selected

of gas after separation from remnant bubbles if bubbles are connected and gas can escape easily from the pyroclasts without changing the vesicular texture.

The range of V_G/V_L (1 to 10^2) is up to more than two orders in magnitude larger than v_g/v_l (0.3 to 5). The fact that the highest V_G/V_L of 10^2 is accounted for by expansion of 0.8 wt% H_2O at atmospheric pressure (0.1 MPa) is suggestive that the amount of gas in the ash plume at the vent was originated largely from separated gas (0.5 wt%) at a little deeper level (< 1 km) within the conduit (Fig. 13). In addition, as V_G/V_L may be underestimated due

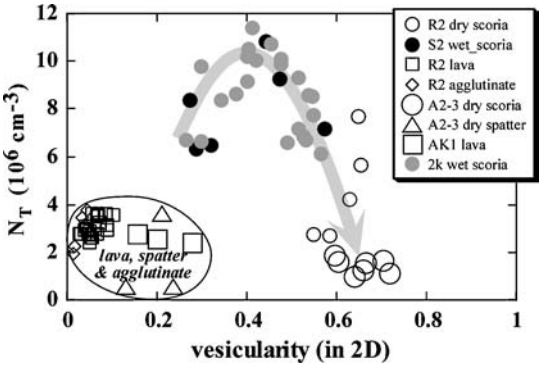

Fig. 11 Variation of the total number density N_T of bubbles with vesicularity. It shows maximum value at $\Phi \sim 0.5$. Lava and spatter have low number density

to poor quality of V_G estimation (factor of 2; Vergniolle and Mangan 2000), the contribution to the plume from the gas separated at deeper level might have been much larger.

It is commonly expected for explosive eruptions that the vesicularity of products represents that of magma at fragmentation level. However, the discrepancies between V_G/V_L and v_g/v_l, and between initial and residual water contents indicate that significant portion of gas phase should have escaped somewhere from magma. Mangan and Cashman (1996) summarized that there are two types of models on the origin of gas phase preserved in pyroclast. Some investigators proposed that magmatic foams form by the accumulation of bubbles in a static layer at the reservoir roof (Vergniolle and Jaupart 1986), and others proposed that foams are formed in the conduit at very shallow depths as magma nearing the surface decompresses (Sparks, 1978). Mangan and Cashman (1996) supported the latter model because of high bubble number density of the products in contrast to static accumulation of bubbles which would result in much lower number density. Our results are also consistent with the latter for the origin of pyroclasts. However, we also suggest that the accumulation of bubbles such as in the former model accounts for the differences between V_G/V_L and v_g/v_l, and between the initial and residual water contents. For the 1991–95 eruption of Unzen dacitic magma, similar discrepancy is accounted

for by degassing along fractured zone between the dike and country rock which was formed by shear (Nakada et al. 2004). In the case of less viscous basaltic magma of Miyakejima, however, existence of such fractured zone is unlikely, and in fact no such fractured zones are observed along vertical cross section of the dike. These observations are also consistent with the idea that significant portion of gas phase has been segregated upward in the less viscous magma as large bubbles leaving magma with small bubbles (scoria).

Degassing processes

It is shown that the scoria are generated by vesiculation at a shallow level during ascent, and thus it is expected that information about the vesiculation process is recorded in remnant bubble textures. We discuss these textures first by focusing on explosive eruptions, and then on effusive eruptions.

Vesiculation process of explosive eruptions

The correlation of vesicularity, residual water content, and BSD pattern of scoria strongly suggest that each piece of scoria represents a snapshot taken during magma ascent. We can therefore determine the vesiculation path of ascending magma in explosive eruptions by investigating the textures of scoria in ascending order of vesicularity.

The most remarkable variation is that total bubble number density N_T has its maximum at vesicularity $\Phi \sim 0.5$ (Fig. 11). When $\Phi < 0.5$, number density increases for both large ($d > 0.1$ mm) and small bubbles ($d < 0.1$ mm) with increase in vesicularity (Fig. 9a). These facts indicate that bubble nucleation is the dominant vesiculation process when vesicularity is below ca. 0.5. In contrast, N_T for vesicular dry scoria ($\Phi > 0.5$) decreases with vesicularity and is lower than that for the most vesicular wet scoria ($\Phi \sim 0.5$). This indicates that vesicularity increases beyond 0.5 mainly due to a small increase in the number density of large bubbles ($d > 0.4$ mm) (as well as in volume fraction; Fig. 7) coincident with coalescence of small bubbles, and also continued bubble growth.

As coalescence of bubbles occurs by thinning and rupture of bubble wall or melt film, melt film thickness may be a good indicator of bubble coalescence. It is not easy, however, to define which part of the melt film represents the structure. Thus here we introduce average bubble radius $\langle r \rangle$ and average melt film thickness $2\langle d \rangle$, where $\langle d \rangle$ is the average thickness of melt shell in the cell models such as in Proussevitch and Sahagian (1998). The average bubble radius,

$$\langle r \rangle = \left(\frac{3\Phi}{4\pi N_T} \right)^{\frac{1}{3}}, \tag{2a}$$

and the average thickness of melt shell of a cell of a bubble,

$$\langle d \rangle = \frac{1}{4\pi \langle r \rangle^2 N_T}, \tag{2b}$$

as N_T is the number density relative to melt volume.

The relationship between $\langle d \rangle$ and vesicularity is shown in Fig. 12 with contours of $\langle r \rangle$. When $\Phi < 0.5$, $\langle r \rangle$ is nearly constant (ca. 15–25 μm) while $2\langle d \rangle$ decreases with vesicularity. At $\Phi \sim 0.5$, $2\langle d \rangle$ is comparable to the minimum unruptured bubble wall thickness (ca. 15–20 μm; Fig. 3c-1). Then $\Phi > 0.5$, $2\langle d \rangle$ and $\langle r \rangle$ suddenly increase up to 25 μm and 50 μm, respectively, indicating intensive bubble coalescence. In fact, nearly all bubbles in scoria are connected ($C^{\#} \sim 1$; Table 4, Fig. 3d-2). These facts are consistent with the interpretation deduced from the changes in BSD.

Small bubbles less than ca. 0.1 mm correspond to those that settled in between larger bubbles in the dry vesicular scoria (Fig. 3a-2). Such small bubbles are dominant in less vesicular wet scoria ($\Phi \sim 0.3$; Fig. 3a-1 and 3c-1). Larger bubbles just touch each other at one or two points (aperture

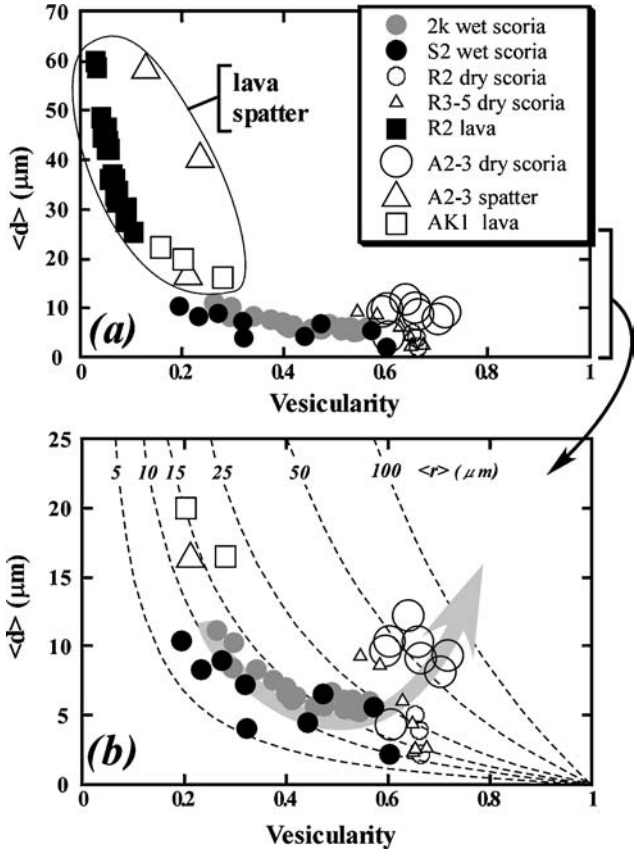

Fig. 12 Vesicularity and average melt shell thickness in the cell model, $\langle d \rangle$, for **a** all samples, and **b** scoria. Broken line indicates isopleth of average bubble radius $\langle r \rangle$. Scoria show almost constant bubble radius with vesicularity increase (film thinning) when $\Phi < 0.5$, while it suddenly increases as well as film thickness at $\Phi \sim 0.5$. The average bubble radius of lava and spatter is nearly constant while film thickens with vesicularity decrease indicating separation of bubbles

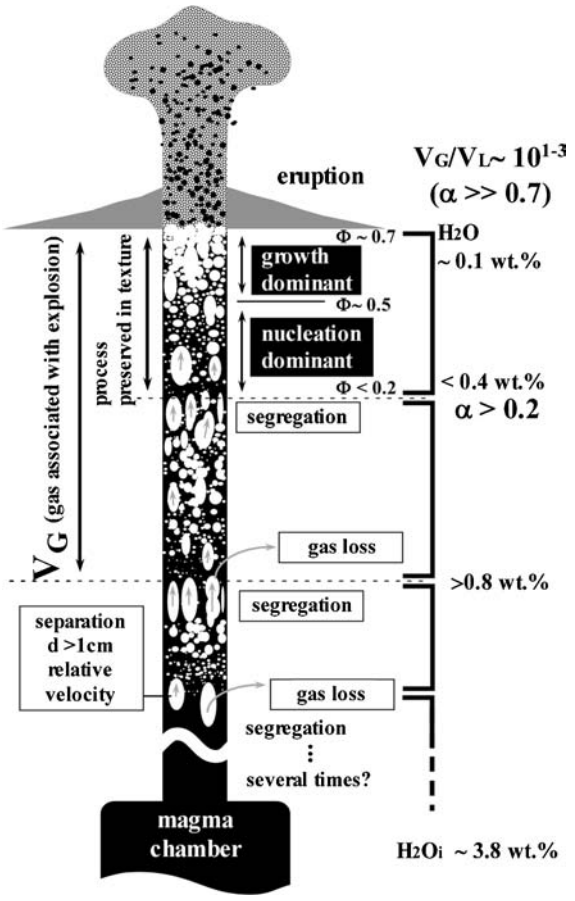

Fig. 13 Schematic illustration of the vesiculation path in the conduit for the explosive eruptions at Miyakejima. At deep level, bubble segregation occurs (possibly several times), and some large bubbles may migrate into upper preceding magma. At shallow level, vesiculation takes place by nucleation until vesicularity reaches $\Phi \sim 0.5$, then by expansion as a consequence of coalescence which may effectively lower the degree of volatile supersaturation and stop further nucleation. α: volume fraction of gas phase in the conduit

size of ca. 1 μm to less than 50 μm) on the bubble wall (Fig. 3d-1). Some bubbles are clustered sometimes to form clots of ca. 1 mm. These features display aspects of snapshots when bubbles just started connecting with each other, and indicate that bubble interaction began at relatively early stages of vesiculation ($\Phi \sim 0.3$) before complete packing.

Consequently, vesiculation paths of magma in the explosive eruptions of the 1983 and 2000 eruptions are divided into two regimes (Fig. 13). The first regime for $\Phi < 0.5$ is dominated by bubble nucleation that lasts until bubbles are extensively connected. The second regime ($\Phi > 0.5$) is dominated by growth and expansion of large bubbles with coalescence of small bubbles. The clear transition in texture may suggest that this transition in vesiculation mechanism was due to a structural change within the magma itself through bubble coalescence rather than a change in external conditions such as super-cooling by seawater. The coalescence is likely to have occurred spontaneously in liquid state because most ruptured melt films are retracted smooth surface, and not by acoustic wave in solid state after eruption. However, acoustic wave such that large bubble exerts when it explodes at the vent might be a candidate that triggers melt rupture in liquid state.

Degassing process of effusive eruptions

In vesicular scoria we observed systematic differences in vesicularity and residual water content (Fig. 6), and in total number density (Fig. 11). In addition, the form of BSD changes gradually from vesicular scoria through spatter to lava flows (Fig. 9b). In terms of texture, large deformed bubbles are observed in dense spatter and lava samples (Fig. 3a-3 and 3b-2). These features indicate that the vesiculation process of effusive eruption was similar to those of explosive eruptions (large bubbles were generated by growth and by coalescence of small bubbles), but also that most large bubbles had been lost by separation with deformation before magma reached the vent. Sparks (1978) argued that, in typical basaltic magma, bubbles less than 1 cm would not be separated during ascent due to very small relative speed to magma. The absence of bubbles larger than 1 cm in spatter and lava flow samples is consistent with our interpretation. Thus we suggest that vesicularity of the products is fundamentally controlled by coalescence and separation of bubbles against growth and expansion at a shallow level.

As it takes a finite time for bubbles to be separated, eruption styles would be affected also by the ascent rate of magma. Eruption speeds of magma (or dense magma flux per unit cross section of vent) observed in effusive and in dry explosive eruptions of Miyakejima were less than 10^{-1} to 10^{0} m/s and more than 10^{-1} to 10^{0} m/s, respectively. If the ascent rate really controls the eruption style, it is likely that sufficient bubble separation occurs when ascent rates are below ca. 10^{-1} to 10^{0} m/s, whereas it does not occur for explosive eruptions where ascent rates exceed 10^{-1} to 10^{0} m/s. Seismic data (Fujita et al. 2001) show that magma-related activity started approximately half a day before the 2000 submarine eruption at the depth of the magma chamber (5–6 km) suggesting an average ascent rate of ca. 10^{-1} m/s. The ascent rate of the 1983 magma at a depth of ca. 100 m at the beginning of eruption is also estimated ca. 0.05–0.1 m/s (Aramaki and Hayakawa 1984; Soya et al. 1984) on the basis of fissure migration rate at different altitudes.

These facts seem to support the idea that intensive dehydration and sufficient gas loss, or upward segregation of large bubbles by flotation, occurred during ascent at deeper levels in the conduit where ascent rate of magma is slow. The segregation occurred possibly several times to account for the large difference between the initial and residual water contents. Then, finally at shallower level near the vent, the eruption styles are controlled by ascent speed because the speed can increase easily due to expansion of gas phase with small amount of water (Fig. 13).

Effect of bubble–bubble interaction

Constraints on vesiculation models

Mangan et al. (1993) suggested that BSD for Hawaiian basaltic scoria follows an exponential law, and adopted a model assuming constant nucleation and growth rates to estimate the ascent rate of magma. Tsukui and Suzuki (1995) measured BSD for bubbles up to 0.5 mm in the products of the 1983 Miyakejima eruption, and also fit an exponential function which truncated at $d \sim 0.2$ mm. They interpreted that small bubbles which form a steeper segment of the curve had been nucleated by sudden super-cooling due to interaction with external water (higher nucleation rate), and that larger bubbles had been nucleated before the interaction (lower nucleation rate). The results of the present study also show that BSD data can be approximately fit by a truncated exponential function (Fig. 8). However, this occurs both for phreatomagmatic and sub-plinian scoria, and for different size ranges (less than 0.4 mm and less than 4 mm; Fig. 8). In addition, some BSDs of highly vesicular scoria might be better fit by a power law than by exponential functions (Fig. 8).

In terms of generation mechanism of BSD, Gaonac'h et al. (1996) showed that BSD for sizes up to centimeters in lava flows of Mt. Etna follows a power law, and explained this by successive bubble coalescence. Blower et al. (2001) also showed that BSDs for some pyroclastics follow a power law, but explained this by multiple occurrences of discrete bubble nucleation events. The results of the present study indicate that the vesiculation process evolves from a nucleation dominant to a growth dominant regime during magma ascent. This strongly suggests that BSD of natural pyroclastics does not record steady state processes with constant rates of nucleation and growth but records competing processes, and that caution should be needed to apply simplified models to estimate variables such as bubble growth and nucleation rates.

The fact that the dominant vesiculation mechanism changes simultaneously with extensive coalescence may imply dependence of vesiculation mechanism on the structure of bubbly magma; The exsolution of volatiles by diffusive growth may become easier than by nucleation, because, due to the pressure decrease by bubble connection with lower ambient pressure, supersaturation at the surface between melt and gas phase of isolate bubbles may become smaller than critical supersaturation sufficient for further nucleation.

Interactions of bubbles and microlites in melt

Gardner et al. (1996) proposed from investigation of natural basaltic pyroclasts formed in plinian eruptions that vesicularity of $\Phi \sim 0.6$ is critical for most bubbles to be connected. This value is smaller than the vesicularity of magma generally assumed at the fragmentation level ($\Phi \sim 0.7$). The present results also indicate that vesicularity of most scoria are below 0.7, and that connection of most bubbles starts at $\Phi \sim 0.3$ and becomes intensive at $\Phi \sim 0.5$. We suggest that bubble connection initiates by clustering or segregation even at $\Phi \sim 0.3$ before the closest packing. The heterogeneity in space distribution of bubble may be a consequence of heterogeneous nucleation due to mineral preference as nucleation site (Hurwitz and Navon 1994), or due to heterogeneous water distribution in melt around pre-existing bubbles (Larsen and Gardner 2000). But coalescence itself can be also a major and effective cause of the heterogeneous bubble space distribution. This effect is well illustrated by the theoretical investigation of Blower (2001).

Finally it is suggested that the presence of microlites is also an important factor controlling the vesiculation path of magma. Melt films in between bubbles of two vesicular scoria with different microlite contents (plagioclase) show different behavior. Microlite-poor melts in between bubbles are ruptured and thus these bubbles are connected (Fig. 3b-1), whereas microlite-rich melts persist in between bubbles because the microlites are bridging melt (Fig. 3a-2) which would have been otherwise ruptured. This indicates that at least some sort of microlites perform as inhibitors of bubble coalescence. Such an effect of small particles is well known in the foam industry and related fields (Proussevitch et al. 1993b), and is considered significantly to modify bulk mechanical properties such as the lifetime of foams. Our preliminary BSD investigation of sub-plinian vesicular scoria of similar composition but without microlites (<10%) shows that total number density is two orders in magnitude less than those of Miyakejima, and that small bubbles are especially depleted in the microlite-poor scoria. These features suggest that, in addition to the bubble–bubble interaction, multiphase (crystal, bubble, and melt) interaction significantly modifies the path of vesiculation and gas loss of magma.

Conclusions

Petrological features of the products of the 1983 and 2000 eruptions at Miyakejima volcano show a homogeneous initial condition of magma (composition, temperature, water content) at the onset of ascent regardless of eruption style. In addition, very low residual water contents (< 0.4 wt%) relative to the initial water contents (3.9±0.9 wt%) in the magma chamber (5–6 km deep) indicate extensive dehydration during ascent. Systematic variation in vesicularity and residual water content of scoria indicates that all the scoria can be explained by exsolution and expansion of ca. 0.3 wt% water suggesting extensive dehydration at a deeper level, and dependence of eruption style on vesiculation and degassing path at a shallow level.

Systematic change of BSD with vesicularity for explosive eruptions suggest that nucleation of bubbles is the dominant process of vesiculation when $\Phi < 0.5$. At $\Phi \sim 0.5$, most bubbles are connected, and for $\Phi > 0.5$, the vesiculation proceeds by expansion of large bubbles with coalescence of small ones. Systematic decrease in residual water content, vesicularity, and bubble number density from scoria to lava

and spatter with decrease in vesicularity also shows that effusive activity is a consequence of bubble coalescence and separation due to slow ascent rate at a shallow level which would otherwise result in explosive eruption.

The effect of microlites on the vesiculation and degassing path may be significant, because microlites bridge melts and impede bubble coalescence, suggesting that evolution of BSD is affected by interactions between bubbles and microlites in melt as well as among bubbles.

Acknowledgements J. Stix, V. Kress, and an anonymous reviewer are thanked for their very fruitful discussion and review. We thank T. Koyaguchi, T. Fujii, K. Kurita, H. Iwamori, and S. Nakashima for critical comments which greatly improved this study. A. Yasuda and M. Ohno are thanked for their advice in EPMA analyses and pycnometry. We also thank T. Wright for his review which greatly improved the manuscript

References

Anderson AT Jr, Newman S, Williams SN, Druitt TH, Skirius C, Stolper E (1989) H_2O, CO_2, Cl, and gas in Plinian and ash-flow Bishop rhyolite, Geology 17:221–225

Aramaki S, Hayakawa Y (1984) Sequence and mode of eruption of the October 3–4, 1983 eruption of Miyakejima. Bull Volcanol Soc Jpn 29:S24–S35 (in Japanese with English abstract)

Aramaki S, Hayakawa Y, Fujii T, Nakamura K, Fukuoka T (1986) The October 1983 eruption of Miyakejima Volcano. J Volcanol Geotherm Res 29:203–229

Blower JD (2001) Factors controlling permeability-porosity relationships in magma. Bull Volcanol 63:497–504

Blower JD, Keating JP, Mader HM, Phillips JC (2001) Inferring volcanic degassing processes from vesicle size distributions. Geophys Res Lett 28:347–350

Cashman KV, Mangan MT (1994) Physical aspects of magmatic degassing II. Constraints on vesiculation processes from textural studies of eruptive products. In Carroll MR, Holloway JR (eds) Volatiles in magmas. Rev Mineral 30:447–478

Endo K, Miyaji N, Chiba T, Sumita M, Sakatsume K (1984) Tephrastratigraphical study on the 1983 Miyake-jima eruption. Bull Volcanol Soc Jpn 29:S184–S207 (in Japanese with English abstract)

Frost BR, Lindsley DH (1993) Equilibria among Fe-Ti oxides, pyroxenes, olivine, and quartz:Part II. Application. Am Mineral 77:1004–1020

Fujita E, Ukawa M, Yamamoto E, Okada Y, Kikuchi M (2001) Volcanic earthquake and tremors associated with the 2000 Miyakejima Volcano eruption. J Geograph Jpn 110:191–203 (in Japanese with English abstract)

Gaonac'h H, Stix J, Lovejoy S (1996) Scaling effects on vesicle shape, size and heterogeneity of lavas from Etna. J Volcanol Geotherm Res 74:131–153

Gardner JE, Thomas RME, Jaupart C, Tait S (1996) Fragmentation of magma during Plinian volcanic eruptions. Bull Volcanol 58:144–162

Geshi N, Shimano T, Chiba T, Nakada S (2002) Caldera collapse during the 2000 eruption of Miyakejima Volcano, Japan Bull Volcanol 64:55–68

Hayakawa Y, Aramaki S, Shirao M, Kobayashi T, Tokuda Y, Tsukui M, Kato T, Takada A, Koyaguchi T, Koyama M, Fujii T, Oshima O, Soya T, Uto K (1984) Pyroclastic fall deposits of the October 3–4, 1983, eruption of Miyakejima volcano. Bull Volcanol Soc Jpn 29:S208–S220 (in Japanese with English abstract)

Housh TB, Luhr JF (1991) Plagioclase-melt equilibria in hydrous systems. Am Mineral 76:477–492

Hurwitz S, Navon O (1994) Bubble nucleation in rhyolitic melts:Experiments at high pressure, temperature, and water content. Earth Planet Sci Lett 122:267–280

Jaupart C, Allegre CJ (1991) Gas content, eruption rate and instabilities of eruption regime in silicic volcanoes. Earth Planet Sci Lett 102:413–429

Johnson MC, Anderson AT, Rutherford MJ (1994) Pre-eruptive volatile contents of magmas. In Carroll MR, Holloway JR (eds) Volatiles in magmas. Rev Mineral 30:281–330

Kaneko T, Yasuda A, Shimano T, Nakada S, Fujii T, Kanazawa T, Nishizawa A, Matsumoto Y (2005) Subaqueous flank eruption preceding the caldera subsidence at the Miyakejima 2000 activity, Japan. Bull Volcanol 67:243–253

Klug C, Cashman KV (1994) Vesiculation of May 18, 1980, Mount St. Helens magma. Geology 22:468–472

Larsen JF, Gardner JM (2000) Experimental constraints on bubble interactions in rhyolite melts: implications for vesicle size distributions. Earth Planet Sci Lett 180:201–214

Lensky NG, Lyakhovsky V, Navon O (2001) Radial variations of melt viscosity around growing bubbles and gas overpressure in vesiculating magmas. Earth Planet Sci Lett 186:1–6

Lindsley D (1983) Pyroxene thermometry. Am Mineral 68:477–493

Liu Y, Zhang Y (2000) Bubble growth in rhyolitic melt. Earth Planet Sci Lett 181:251–264

Lofgren GE (1980) Experimental studies on the dynamic crystallization of silicate melts. In: Hargraves RB (ed) The Physics of Magmatic processes, Princeton University Press, Princeton, 487–551 pp

Mangan MT, Cashman KV (1996) The structure of basaltic scoria and reticulate and inferences for vesiculation, foam formation, and fragmentation in lava fountains. J Volcanol Geotherm Res 73:1–18

Mangan MT, Cashman KV, Newman S (1993) Vesiculation of basaltic magma during eruption. Geology 21:157–160

Mertzbacher C, Eggler DH (1984) A magmatic geohygrometer:application to Mount St. Helens and other dacitic magmas. Geology 12:587–590

Miyagi I, Matsubaya O, Nakashima S (1998) Change in D/H ratio, water content and color during dehydration of hornblende. Geochem J 32:33–48

Moore G, Vennemann T, Carmichael ISE (1998) An empirical model for the solubility of H_2O in magmas to 3 kilobars. Am Mineral 83:36–42

Nakada S, Yoshimoto M, Shimano T, Kurokawa M, Nakai S, Sugimoto T, Hoshizumi H, Oguri K, Noguchi S, Goto Y (2004) Petrology of conduit lava at Unzen volcano; result of Unzen scientific drilling project. EOS Trans AGU 85(47), Fall Meet Suppl, Abstract V33D–1492

Nakada S, Nagai M, Kaneko T, Nozawa A, Suzuki-Kamata K (2005) Chronology and products of the 2000 eruption of Miyakejima volcano. Bull Volcanol 67:205–218

Proussevitch AA, Sahagian DL (1998) Dynamics and energetics of bubble growth in magmas:Analytical formulation and numerical modeling. J Geophys Res 103:18223–18251

Proussevitch AA, Sahagian DL, Anderson AT (1993a) Dynamics of diffusive bubble growth in magmas:Isothermal case. J Geophys Res 98:22283–22307

Proussevitch AA, Sahagian DL, Kutolin VA (1993b) Stability of foams in silicate melts. J Volcanol Geotherm Res 59:161–178

Rutherford MJ, Devine JD (1996) Preeruption pressure-temperature conditions and volatiles in the 1991 dacitic magma of Mount Pinatubo. In: Newhall CG, Punongbayan RS (eds) Fire and mud:eruptions and lahars of Mount Pinatubo, Philippines. University of Washington Press, Seattle, 751–766 pp

Sahagian DL, Proussevitch AA (1998) 3D particle size distributions from 2D observations:stereology for natural applications. J Volcanol Geotherm Res 84:173–196

Sasaki T, Katsui Y (1981) Pycnometry of pumice by using glass beads. Bull Volcanol Soc Jpn 26:117–118 (in Japanese)

Schmitt AK, De Silva SL (2000) The Mertzbacher & Eggler (1984) geohygrometer: a cautionary note on its suitability for high-K suites. J Petrol 41:357–362

Soya T, Uto K, Suto S (1984) The products of the 1983 eruption of the Miyakejima volcano – with special reference to the lava flow. Bull Volcanol Soc Jpn 29:S220–S241 (in Japanese with English abstract)

Sparks RSJ (1978) The dynamics of bubble formation and growth in magmas – a review and analysis. J Volcanol Geotherm Res 3:1–37

Sumita M (1985) Ring-shaped cone formed during the 1983 Miyakejima eruption. J Volcanol Soc Jpn 30:11–32 (in Japanese)

Toramaru A (1990) Measurement of bubble size distributions in vesiculated rocks with implications for quantitative estimation of eruptive process. J Volcanol Geotherm Res 43:71–90

Toramaru A (1995) Numerical study of nucleation and growth of bubbles in viscous magmas. J Geophys Res 100:1913–1931

Tsukui M, Suzuki Y (1995) Vesiculation of basaltic magma:magmatic versus phreatomagmatic eruptions in 1983 eruption of Miyakejima. Bull Volcanol Soc Jpn 40:395–399 (in Japanese)

Tsukui M, Niihori K, Kawanabe Y, Suzuki Y (2001) Stratigraphy and formation of Miyakejima Volcano. J Geograph Jpn 110:156–167 (in Japanese with English abstract)

Turek A, Riddle C, Cozens BJ, Tetley NW (1976) Determination of chemical water in rock analysis by Karl Fischer titration. Chem Geol 17:261–267

Ueki S, Shimizu H, Koyama J, Takagi A (1984) Seismic activity following the 1983 eruption of Miyakejima. Bull Volcanol Soc Jpn 29:S68–S80 (in Japanese with English abstract)

Vergniolle S, Jaupart C (1986) Separated two-phase flow and basaltic eruptions. J Geophys Res 91:12842–12860

Vergniolle S, Mangan M (2000) Hawaiian and Strombolian eruptions. In: Sigurdsson H, Houghton B, McNutt SR, Rymer H, Stix J (eds) Encyclopedia of Volcanoes, Academic Press, 447–461

Westrich HR (1987) Determination of water in volcanic glasses by Karl-Fischer titration. Chem Geol 63:335–340

Woods A, Koyaguchi T (1994) Transitions between explosive and effusive eruptions of silicic magmas. Nature 370:641–644

Yasuda A, Nakada S, Fujii T (2001) Sulfur abundance and redox state of melt inclusions from Miyake-jima 2000 eruption products. Bull Volcanol Soc Jpn 46:165–173 (in Japanese with English abstract)